Theoretical Investigation of Mechanisms for the Gas-Phase Unimolecular Decomposition of DMMP

Li Yang,[†] Robert M. Shroll,[‡] Jiaxu Zhang,[†] U. Lourderaj,[†] and William L. Hase*,[†]

Department of Chemistry and Biochemistry, Texas Tech University, Lubbock, Texas 79409, and Spectral Sciences, Incorporated, 4 Fourth Avenue, Burlington, Massachusetts 01803-3304

Received: May 6, 2009; Revised Manuscript Received: October 2, 2009

All species involved in the multichannel decomposition of gas-phase dimethyl methylphosphonate (DMMP) were investigated by electronic structure calculations. Geometries for stationary structures along the reaction paths, were fully optimized with the MP2 method and the B3LYP and MPW1K DFT functionals, and the 6-31G*, 6-31++G**, and aug-cc-pVDZ basis sets. The geometries determined by the B3LYP and MPW1K functionals are in very good agreement with the MP2 values. Increasing the basis set size from 6-31G* to aug-cc-pVDZ does not significantly alter this result. Single point energy calculations were carried out with highly accurate but computationally more expensive CBS-QB3 theory. DMMP has three conformers, which lead to the four primary product channels, (O)P(CH_2)(OCH_3) + CH_3OH, (O)P(CH_3) (OCH_3)(OH) + CH_2, c-(O)P(CH_3)OCH_2 + CH_3OH, and (O)P(CH_3)(OCH_3)(OCH) + H_2. The first channel has the lowest energy barrier and is expected to be the most important pathway. It occurs via C−H and P−O bond cleavages accompanied by O−H bond formation. The other three channels have higher and similar energy barriers, and are expected to have smaller and similar rates. The product (O)P(CH_3)(OCH_3)(OCH) undergoes a secondary decomposition to form (OH)P(CH_3)(OCH_3) + CO.

I. Introduction

The decomposition of organophosphorus compounds has been of interest for several years, primarily for understanding the destruction of chemical warfare agents (CWAs).[1−22] Such organophosphorus materials are extremely toxic nerve and blistering agents, and include Soman (GD), Sarin (GB), and VX. Since the testing of CWAs in the laboratory is quite hazardous, typically, studies are done using less toxic simulants. Dimethyl methylphosphonate (DMMP) is often used to simulate the chemical and structural properties of toxic organophosphorus compounds,[7−12] because of its similarity in physical and chemical properties to CWAs. DMMP, GB, and VX conform to the structure

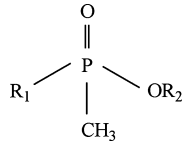

where R_1 and R_2 are differing functional groups. For DMMP, $R_1 = OCH_3$ and $R_2 = CH_3$; for GB, $R_1 = F$ and $R_2 = CH(CH_3)_2$; and for VX, R1 = $SCH_2CH_2N(C_3H_7)_2$, and $R_2 = CH_2CH_3$. DMMP is a liquid at 298 K, having a low vapor pressure of 1.05 Torr.[9] The P−O and P−C bonds in DMMP are less reactive than P−F bonds in actual nerve agents. DMMP is employed by many experimentalist to predict the chemical reactivity of Sarin. A detailed understanding of the complex chemistry of DMMP decomposition is necessary to better interpret the experimental efforts and to make accurate connections with the reactivity of CWAs.

There are different methods for decomposing DMMP. An important area of chemical warfare agent destruction is catalytic decomposition using metals and metal oxides. Previous DMMP-substrate research involved Rh(100),[13] Mo(111),[7] Pt(111),[14] Pd(111),[15] TiO_2,[16,17] Al_2O_3,[10,18,23−25] SiO_2,[11,26] Fe_2O_3,[12] MgO,[19,20] Y_2O_3,[21] and alumina-supported iron oxide.[22] A kinetic model has been developed for the decomposition of DMMP in a hydrogen/oxygen flame.[27] Ab initio calculations have been performed to study the alkaline hydrolysis of the nerve agents paroxon[28] and sarin,[29] but apparently there are no similar studies for DMMP. In fact, there appear to be no previous investigations of DMMP unimolecular decomposition in any medium or environment.

In the current paper, we carry out a detailed theoretical study of the potential energy surface (PES) for the gas-phase unimolecular decomposition of DMMP using different levels of theory to (1) establish the isomerization and dissociation unimolecular pathways for DMMP and (2) to investigate the methods required to accurately describe DMMP unimolecular decomposition.

II. Computational Method

The unimolecular decomposition reaction of DMMP was examined at a variety of theoretical levels, since there are no previous evaluations of computational methods or experimental data for this system. All of the critical structures (equilibria and transition states) for the different decomposition pathways were fully optimized using second-order Møller−Plesset perturbation theory (MP2)[30] and two hybrid density functional theory (DFT) methods, that is, the Becke three-parameter Lee−Yang−Parr (B3LYP)[31] and modified Perdew−Wang one-parameter model for kinetics (MPW1K).[32] MPW1K has been specifically designed for accurate but tractable computations of barrier heights and saddle point geometries. In this hybrid functional, the proportion of Hartree−Fock exchange has been significantly increased compared with the more traditional B3LYP. A

* Corresponding author. E-mail: bill.hase@ttu.edu.
[†] Texas Tech University.
[‡] Spectral Sciences, Incorporated.

10.1021/jp904232n CCC: $40.75
Published on Web 11/10/2009

comparison of basis set effects on geometries was also performed by using the three different basis sets 6-31G*, 6-31++G**, and aug-cc-pVDZ[33] for the B3LYP, MPW1K, and MP2 calculations. Harmonic vibrational frequencies were calculated using the above methods with the aug-cc-pVDZ basis set, to compare the frequencies calculated at different levels of theory and to check whether an obtained stationary point is a minimum (with all real frequencies) or a transition state (with a single imaginary frequency). For each transition state, the intrinsic reaction coordinate (IRC)[34] was calculated for both directions off the saddle point, at the B3LYP/6-31G* level, to guarantee its correct connection to the designated minima. Finally, to obtain more reliable energies, higher level CBS-QB3[35] calculations were performed for all stationary points using the B3LYP/aug-cc-pVDZ geometries. The NWChem[36] computer program was used to perform most of the above electronic structure calculations. Gaussian03[37] was used to calculate the IRCs.

The MP2 optimizations were performed using the tight convergence criteria and for the DFT calculations the convergence criteria were set to: convergence energy 1.0×10^{-7}, convergence density 1.0×10^{-6}, and convergence gradient 1.0×10^{-6}, ensuring adequate convergence and the reliability of the computed frequencies, especially those for the low-frequency modes. For the same reason, the xfine grid was specified for the DFT calculations.

III. Results and Discussion

Figure 1 depicts structures of all reactants, products, isomers (Isom's), intermediates (Im's), and transition states (TS's) obtained for the unimolecular decomposition of DMMP, at the B3LYP/aug-cc-pVDZ level of theory. To test the influence of the methodology and basis set size on the calculated geometries, geometries of all stationary points were optimized at the B3LYP, MPW1K, and MP2 levels of theory using the 6-31G*, 6-31++G**, and aug-cc-pVDZ basis sets. The geometries determined for conformer I and TS3, the lowest energy TS, with the different levels of theory are listed in Table 1. The remaining geometries are listed in Supporting Information, Table S1. Figure 2 gives histograms of differences of bond distances (left) and bond angles (right) between the different basis sets.

Four products containing phosphorus, P1−P4, are formed by the primary decomposition of DMMP. A fifth product, P5, is formed by a secondary decomposition of P4. The molecular formulas for these products are

P1 $(O)P(CH_2)(OCH_3)$

P2 $(O)P(CH_3)(OCH_3)(OH)$

P3 $c\text{-}(O)P(CH_3)OCH_2$

P4 $(O)P(CH_3)(OCH_3)(OCH)$

P5 $(OH)P(CH_3)(OCH_3)$

Vibrational frequencies for all stationary points were calculated with B3LYP, MPW1K, and MP2 using the aug-cc-pVDZ basis set. The different levels of theory give similar vibrational frequencies except for the lowest values. This is illustrated in Figure 3 and Table 2. Figure 3 compares the computed frequencies for conformer I with the experimental values[8] in terms of the relative uncertainty $[\nu_{exp}(i) - \nu_{calc}(i)]/\nu_{exp}(i)$ for each ith vibrational mode. Table 2 compares the frequencies calculated for conformer II and TS3. These two structures were chosen since conformer II has the lowest vibrational frequencies and TS3 is the lowest energy TS. The calculated vibrational frequencies are listed in Supporting Information, Table S2 for all stationary points. As discussed above, the xfine grid was used for the frequency calculations. A scaling factor was not used to adjust the calculated harmonic frequencies to experimental anharmonic values.

To test the reliability of the frequency calculations, different levels of accuracy of numerical integration, that is, default, fine, and xfine, were used to calculate the frequencies at the B3LYP/aug-cc-pVDZ level of theory for conformers I and II, isomer 1 (Isom1), and intermediate 1 (Im1), which have low frequencies. The largest frequency differences calculated, using these three levels of accuracy, lie in the lowest four frequencies. In general, most of the low frequencies are insensitive to the DFT grid settings, but for some of the low frequencies, it is necessary to use more grid points. The largest difference between the default and the fine frequencies for conformers I and II, Isom1 and Im1 is 5, 8, 4, and 8 cm^{-1}, respectively. For the fine and xfine frequencies, these respective differences are smaller and 2, 3, 3, and 2 cm^{-1}. The largest percentage difference between the frequency values is for a conformer II extremely low vibrational frequency, which is 22 and 14 cm^{-1} for the default and fine grids, respectively. With the xfine grid, this frequency is 12 cm^{-1}.

Table 3 displays the relative energies for the stationary points calculated with B3LYP, MPW1K, and MP2 using the aug-cc-pVDZ basis set. CBS-QB3 energies were chosen as a benchmark for the accuracy of the calculations and were compared with energies calculated at the above levels of theory. For convenient comparisons, the energy of DMMP conformer I, which has the lowest energy, is set to zero. A schematic reaction coordinate PES diagram is given in Figure 4, which illustrates the connection of the different stationary points by their IRCs. The energies included are the CBS-QB3 values.

In the following details of the structures, vibrational frequencies, and energies of the stationary points are presented, as well as properties of the decomposition mechanisms. Also included are comparisons of the different theoretical methods.

A. Conformers and Isomers of DMMP. A search of the DMMP PES was carried out at the B3LYP/6-31G* level of theory using 10 starting geometries involving different orientations of the methoxy groups. Six equilibrium geometries were obtained by these calculations, referred to as conformers I−IV and isomers 1 and 2 (Isom1 and Isom2), and they remained after a second set of calculations using MP2/aug-cc-pVDZ theory. Their CBS-QB3 relative energies are depicted in Figure 4.

Conformer I has the lowest energy, and it can readily interconvert to conformers II−IV through an internal rotation about the P−O bond. Though, conformer I has a totally asymmetric geometry with inequivalent methoxy groups and conformer II has a plane of symmetry, they are nearly isoenergetic, with conformer II only 0.4 kcal/mol higher in energy. Conformers III and IV are enantiomorphous and have an asymmetric geometry with two methyl groups located on the opposite sides of the PO2O3 plane. They lie 1.9 kcal/mol higher in energy than conformer I. None of the intrinsic reaction coordinates (IRCs)[32] found in this work, which connect DMMP with its unimolecular decomposition products, involved conformer IV.

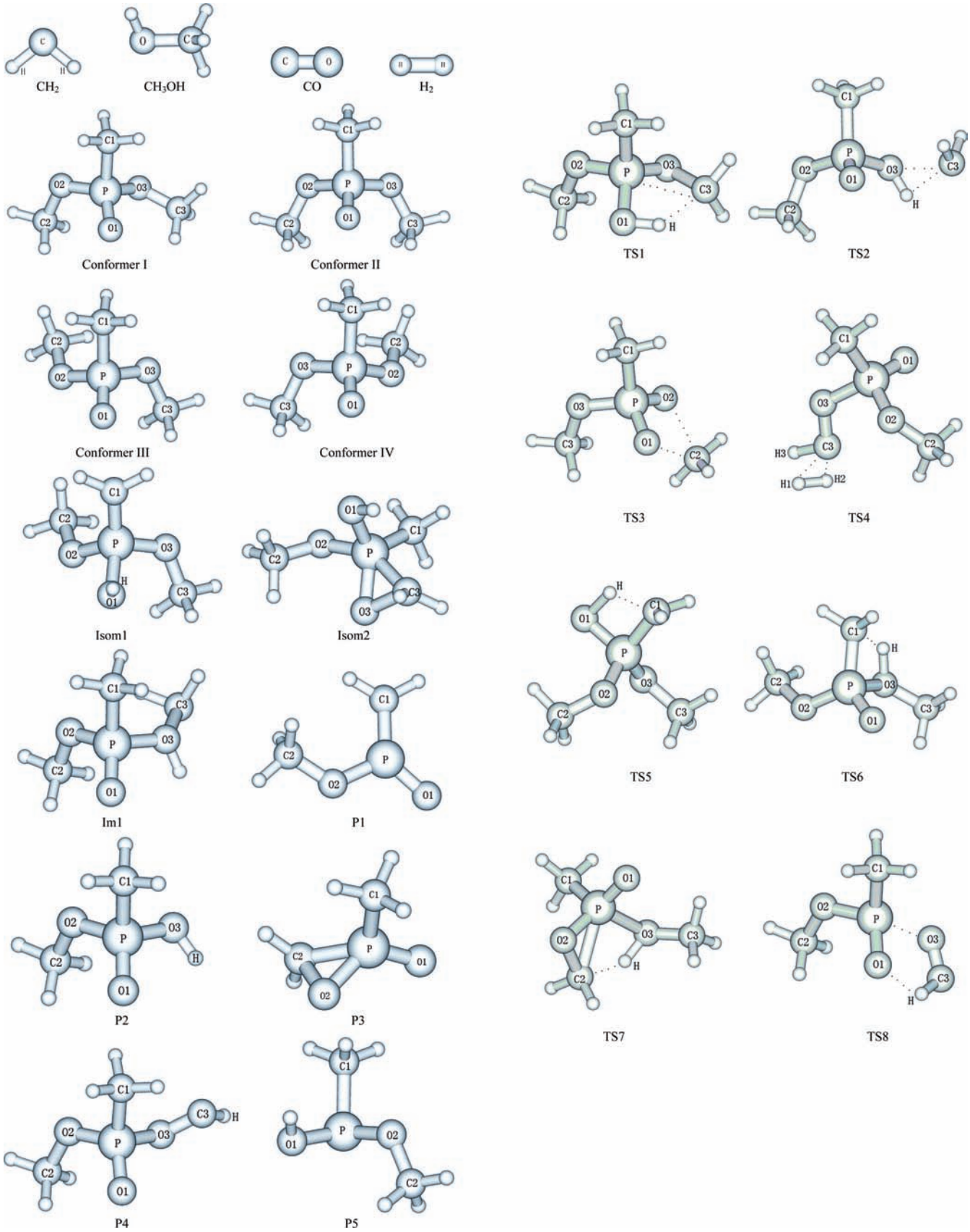

Figure 1. Stationary point geometries optimized at the B3LYP/aug-cc-pVDZ level of theory with identifying labels.

Isomers 1 and 2 are higher energy structures. For Isom1, a H atom is transferred from the $-CH_3$ group to the O atom of the P═O bond. For Isom2, a H atom is transferred from one of the $-OCH_3$ groups to the O atom of P═O, resulting in a $POCH_2$ three-membered ring. No reaction paths were found between these isomers and the possible products.

A previous rotational spectroscopy and ab initio study of DMMP considered its structure.[38] Ab initio calculations carried

TABLE 1: Geometries Determined for Conformer I and TS3 with Different Levels of Theory

	B3LYP			MPW1K			MP2		
	6-31G*	6-31++G**	aug-cc-pVDZ	6-31G*	6-31++G**	aug-cc-pVDZ	6-31G*	6-31++G**	aug-cc-pVDZ
Conformer I									
R_{P-O1}	1.49	1.49	1.51	1.47	1.47	1.48	1.49	1.50	1.51
R_{P-O2}	1.62	1.62	1.64	1.59	1.59	1.61	1.61	1.61	1.63
R_{P-O3}	1.63	1.63	1.65	1.61	1.61	1.62	1.63	1.63	1.65
R_{P-C1}	1.81	1.81	1.81	1.79	1.79	1.79	1.80	1.79	1.80
$\theta_{O1-P-C1}$	116.6	116.4	116.8	116. 7	116.5	116.7	116.7	116.5	116.6
$\theta_{O1-P-O2}$	117.2	116.8	117.0	116.8	116.4	116.6	117.4	117.2	117.4
$\theta_{O1-P-O3}$	113.9	113.4	113.7	113.4	113.0	113.4	113.7	113.3	113.8
$\theta_{P-O2-C2}$	118.8	119. 7	118.3	118.5	119.2	117.8	117.0	117.8	115.5
$\theta_{P-O3-C3}$	120.0	120.4	119.3	120.0	120.4	118.9	117.9	118.4	116.1
$\theta_{O2-P-O3}$	101.3	101. 7	101.0	101.6	101.9	101.2	101.0	101.2	100.4
TS3									
R_{O1-C2}	2.13	2.16	2.15	2.08	2.10	2.10	2.07	2.09	2.08
R_{O2-C2}	2.13	2.16	2.15	2.07	2.10	2.10	2.07	2.09	2.08
R_{P-O1}	1.54	1.54	1.56	1.52	1.52	1.52	1.54	1.55	1.57
R_{P-O2}	1.54	1.54	1.56	1.52	1.52	1.52	1.54	1.55	1.57
R_{P-O3}	1.63	1.63	1.65	1.61	1.61	1.61	1.63	1.63	1.66
R_{P-C1}	1.81	1.81	1.81	1.79	1.79	1.79	1.80	1.79	1.81
R_{O3-C3}	1.43	1.43	1.43	1.41	1.41	1.41	1.44	1.44	1.45
$\theta_{P-O1-C2}$	91.1	91.8	91.6	91.2	91.7	91.8	90.7	91.1	91.0
$\theta_{P-O2-C2}$	91.0	91.6	91.6	91.4	91.7	91.6	90.7	91.1	91.0
$\theta_{O1-P-C1}$	113.0	113.2	113.7	113.5	113.6	113.6	113.6	113.8	114.4
$\theta_{O1-P-O2}$	106.8	106.6	106.0	113.5	105.8	105.8	105.4	105.3	104.4
$\theta_{O1-P-O3}$	112.2	112.1	112.1	112.1	120.0	112.0	112.4	112.2	112.3
$\theta_{P-O3-C3}$	118.6	119.6	118.2	118.2	119.0	119.0	116.6	117.3	115.0
$\theta_{O2-P-O3}$	112.2	112.1	112.1	112.1	111.9	111.9	112.4	112.2	112.3

out at both the HF/6-31G* and the MP2/6-311G* levels of theory indicated there may be as many as three possible low-energy gas-phase conformations at 300 K, similar to what we find. However, they did not identify conformer IV. By comparing their ab initio-calculated structures with the experimental data, they concluded that the conformer that best models the experimental results is the lowest energy conformer I.

B. Intermediates, Transition States, and Products. ***1. Geometries.*** Figure 2 shows the differences in the stationary point geometries of changing the basis set from 6-31G*, 6-31++G** to aug-cc-pVDZ, for B3LYP, MPW1K, and MP2, respectively. The differences of bond distances and bond angles between the basis sets, that is, (aug-cc-pVDZ)-(6-31G*), (aug-cc-pVDZ)-(6-31++G**), and (6-31++G**)-(6-31G*), are reported in histograms for B3LYP, MPW1K, and MP2, and each histogram is fit with the normal distribution of error curve. The position of the maximum of the normal distribution of error curve corresponds to the mean deviation of the error while the half-width at half-maximum reflects the scattering of the error's standard deviation. The average values of the (aug-cc-pVDZ)-(6-31G*), (aug-cc-pVDZ)-(6-31++G**), and (6-31++G**)-(6-31G*) normal distribution curves for B3LYP (MPW1K, MP2), are 0.011 (0.007, 0.009), 0.008 (0.007, 0.009), and 0.003 (−0.005, −0.0004) Å, respectively, and their respective standard deviations are 0.024 (0.022, 0.026), 0.016 (0.014, 0.019), and 0.014(0.014, 0.014) Å. In general, changing the basis set results in only small differences in bond distances for each of the three methods, and the differences of the bond lengths are generally less than 0.05 Å. The largest differences, around 0.1 Å, lie in C3−H2 in TS4, C3−H1 in TS2, and O3−C3 in Im1. For all three methods, the means of (aug-cc-pVDZ)-(6-31G*) and (aug-cc-pVDZ)-(6-31++G**) are statistically close and larger than the means of (6-31++G**)-(6-31G*). The standard deviations have the same trend, which means aug-cc-pVDZ gives slightly different bond distances as compared with 6-31++G** and 6-31G*.

Now consider the effects of changing the basis sets on bond angles. As shown in Figure 2, the average values of the (aug-cc-pVDZ)-(6-31G*), (aug-cc-pVDZ)-(6-31++G**), and (6-31++G**)-(6-31G*) normal distribution curves for B3LYP (MPW1K, MP2), are −0.24 (−0.24, −0.58), −0.35 (−0.39, −0.66), and 0.11 (0.15, 0.08)°, respectively, and their respective standard deviations are 1.34 (0.96, 1.32), 1.15 (0.93, 1.51), and 1.02 (1.03, 1.02)°. For all three methods, 6-31++G** and 6-31G* give relatively similar bond angles, and they have opposite systematic errors as compared with aug-cc-pVDZ. The standard deviations are statistically the same when varying the basis sets. The differences of the bond angles are generally less than 2°, and the most important change observed in the geometry with increase in the basis set size, for each of the three methods, corresponds to the angles of P−O3−C3 for Im1 and TS2. In addition, the B3LYP/aug-cc-pVDZ O1−P−O2 and O1−P−O3 bond angles in Isom1 differ by 3.7° and 3.4°, respectively, from the B3LYP values obtained with the 6-31++G** basis set. For the same angles in Isom1, MP2/aug-cc-pVDZ also differs around 4.5° from those obtained with other two basis sets. The B3LYP/aug-cc-pVDZ H1−C3−H2 bond angle in TS4 is 31.3°, and larger than 25.6° obtained by B3LYP/6-31G*.

In general, the B3LYP, MPW1K, and MP2 stationary point structures with aug-cc-pVDZ are in very good agreement. The calculated geometries with the two different functionals, B3LYP and MPW1K, are only slightly different. The bond distances change by 0.1 Å or less, and bond angles change by 2.5° or less. Variations in the bond lengths obtained by the DFT and MP2 methods are less than 0.2 Å, and variations in the bond angles are 4° or less, except for the angle of P−O3−C3 of Im1, TS2, and TS6, for which the differences between B3LYP and MP2 are as large as 5.9, 5.4, and 5.1°, respectively. In addition, for the bond angle P−O1−H1 of TS1, the difference between B3LYP and MP2 is 5.0°.

2. Vibrational Frequencies. The gas-phase vibrational spectrum of DMMP has been measured by Cuisset and co-workers[8] and is compared with the harmonic B3LYP, MPW1K, and MP2 vibrational frequencies of the lowest energy conformer I in Figure 3. Figure 3 illustrates that most of the experimental

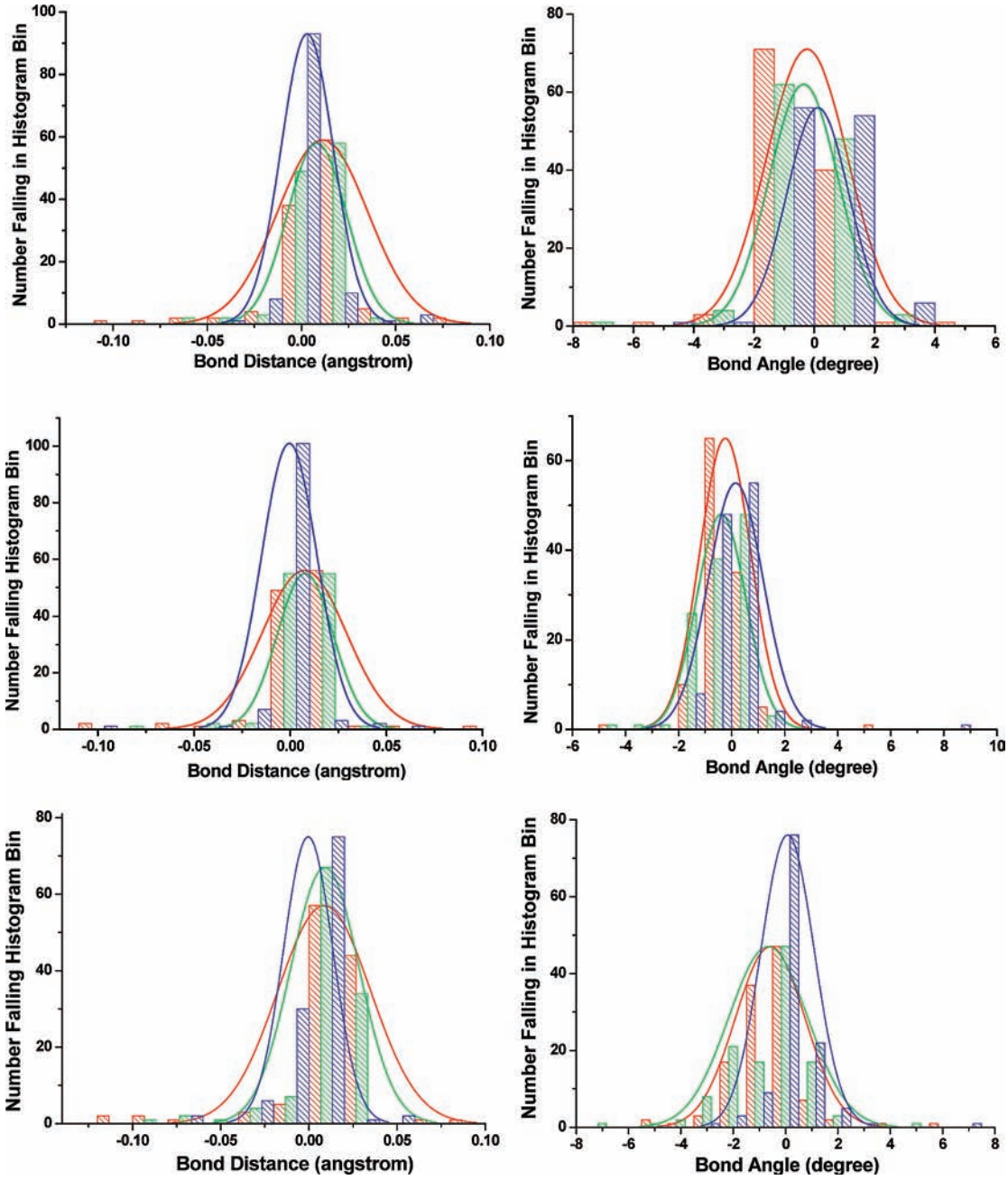

Figure 2. Histograms of differences of bond distances (left) and bond angles (right) between different basis sets, that is (aug-cc-pVDZ)-(6-31G*) (red color), (aug-cc-pVDZ)-(6-31++G**) (green color), and (6-31++G**)-(6-31G*) (blue color) for B3LYP (a), MPW1K (b), and MP2 (c). 116 bond lengths and 118 bond angles for B3LYP, MPW1K, and MP2 are included in each of the histograms and each is fit with the normal distribution of error curve. The fitting parameters are given in the text.

frequencies are predicted by the calculations with a relative uncertainty lower than 10%, except for the lowest frequencies obtained by B3LYP and MP2 for which the relative uncertainties are around 15% and 12%, respectively. For the three modes with $\nu_{exp}(i) > 1600$ cm^{-1}, B3LYP gives the best agreement with experimental frequencies with relative uncertainties of approximately 5%. For the modes with 850 cm^{-1} $< \nu_{exp}(i) <$ 1600 cm^{-1}, the relative uncertainties obtained by B3LYP are smaller than 1%, except for the experimental frequencies of 1275 and 1521 cm^{-1} with relative uncertainties of 5% and 3%. For this spectral region, the frequencies calculated with MP2 are close to those obtained by B3LYP, while MPW1K gives relatively large relative uncertainties. Within the low-frequency part of the vibrational spectrum ($\nu_{exp}(i) < 850$ cm^{-1}), MPW1K gives smaller relative uncertainties than do B3LYP and MP2.

3. Energies. *a. CBS-QB3 Energies.* To obtain more reliable energies beyond the MP2 and DFT results, energy calculations were also performed with the CBS-QB3 multilevel method, which employs nonlinear pair natural orbital extrapolations to the complete basis set limit.[33] First, consider the energies of the conformers, isomers, intermediates, and products. As shown in Table 3, the MP2, MPW1K, and B3LYP energies for the DMMP conformers and Im1 are in good agreement with the CBS-QB3 values. For P1, P3, and P5, MP2 and MPW1K give a better relative accuracy than does B3LYP, when compared with CBS-QB3. However, for P2 and P4, the CBS-QB3 energies are much lower than those of MP2 and MPW1K. For most of the transition states, the CBS-QB3 energies are closer to the B3LYP values and lower than the MPW1K and MP2 energies. The difference in this trend is for TS6 and TS7, whose CBS-

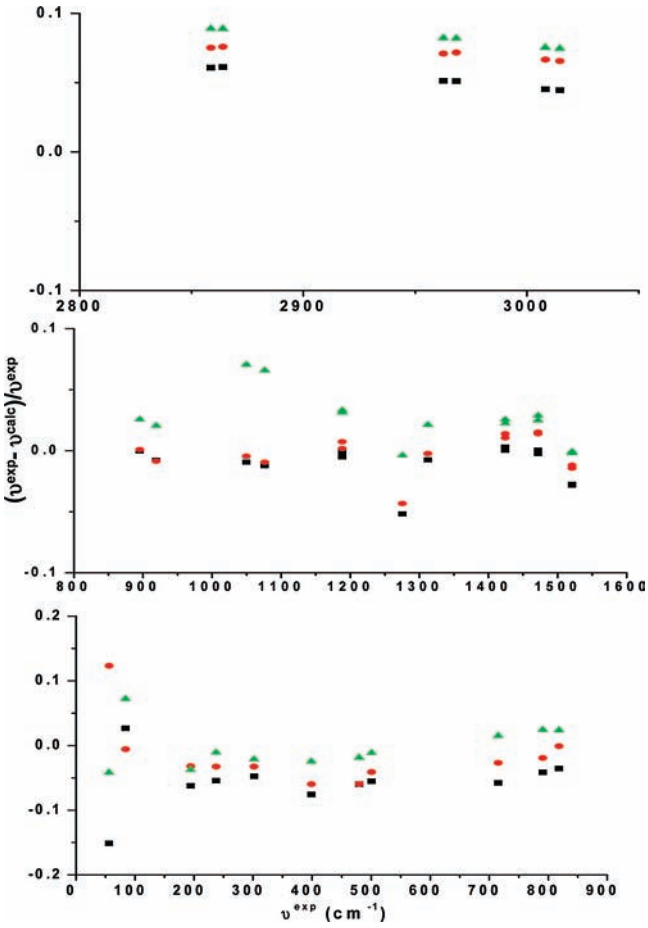

Figure 3. Calculated vibrational frequencies of conformer I of DMMP compared to the anharmonic experimental frequencies.[8] Relative uncertainties for three different levels of theory are plotted as a function of the frequencies of the modes. Squares, circles, and triangles are associated with the harmonic frequencies calculated with B3LYP, MP2, and MPW1K using the aug-cc-pVDZ basis set.

QB3 energies are closer to the MPW1K energies, and are 5.8 and 5.2 kcal/mol higher, respectively, than the B3LYP energies. For TS8, the CBS-QB3 energy is much closer to the MP2 energy than DFT energies.

b. MP2 and DFT Energies. The relative energies found with the B3LYP, MPW1K, and MP2 levels of theory, using the aug-cc-pVDZ basis set, as compared with the CBS-QB3 energies are shown in Figure 5. Nineteen different stationary point energies are included in the histograms, and each is fit with the normal distribution of error curve. The average values of the B3LYP, MPW1K, and MP2 normal distribution curves are −2.4, 2.9, and 1.0 kcal/mol, respectively. Their respective standard deviations are 4.6, 6.2, and 4.9 kcal/mol.

MP2 theory gives a relatively smaller systematic error than do the B3LYP and MPW1K theories. The means between B3LYP and MPW1K are different and have opposite systematic errors. The standard deviations of B3LYP and MPW1K are not statistically different, which means B3LYP and MPW1K are of similar accuracy. Each of these methods suffers from species being found in the highly chemically significant tails of the distributions. As shown in Table 3, the principal differences between the B3LYP and the MP2 energies are for the products. For P1−P5, the B3LYP energies are higher than the MP2 energies by 8.5, 5.7, 6.2, 4.9, and 5.7 kcal/mol, respectively, whereas the energy differences between MPW1K and MP2 are only 0.2, 0.4, 2.4, 2.7, and 7.1 kcal/mol for these products. For TS8, the difference between B3LYP and MPW1K reaches 22 kcal/mol, with the latter apparently much too high.

C. Isomerization and Dissociation Pathways. ***1. Reactions Derived from Conformer I.*** As shown in Figure 4, there are the two reaction paths from conformer I

$$\text{Path 1: Conformer I} \rightarrow \text{TS1} \rightarrow \text{Isom2}$$

$$\text{Path 2: Conformer I} \rightarrow \text{TS2} \rightarrow \text{Im1} \rightarrow \text{P2} + CH_2$$

The first path involves DMMP isomerization to Isom2 via TS1. In TS1, a 1,3 H shift from the C atom of OCH_3 to the O atom of P═O is associated with concerted O−H bond formation and P atom and C atom ring closure, to form the PCO three-membered ring for Isom2. The CBS-QB3 barrier for this process is 62.9 kcal/mol.

For path 2, a migration of a H atom from a C atom to an O atom first forms intermediate Im1. The resulting elongation of the O−C bond varies from 0.27 Å to 0.32 Å for the different calculations. Im1 then dissociates to form P2 and CH_2. For this dissociation process, no transition state was found. To further confirm the absence of a barrier, a pointwise potential curve at the B3LYP/aug-cc-pVDZ level was calculated as shown in Figure 6. For each fixed O−C bond length, the remaining internal coordinates were optimized. Thus, this addition process is a barrierless association.

2. Reactions Derived from Conformer II. Two reactions occur from conformer II; that is

$$\text{Path 3: Conformer II} \rightarrow \text{TS3} \rightarrow \text{Conformer II}$$

$$\text{Path 4: Conformer II} \rightarrow \text{TS4} \rightarrow \text{P4} + H_2$$

$$\text{P4} \rightarrow \text{TS8} \rightarrow \text{P5} + \text{CO}$$

For path 3, the CH_3 group shifts between two oxygen atoms, O1 and O2, with a 58.7 kcal/mol barrier. Path 4 is a 1,1-HH elimination reaction first leading to the products H_2 and P4. The P−O−C−H dihedral angle in P4 is slightly nonplanar with a value of 176.1°. In a secondary dissociation, P4 dissociates via TS8 to give the products CO and P5 via a 1,3 H shift from a C atom to an O atom accompanied by P−O bond cleavage. TS8 has a loose POCHO five-membered planar ring structure. At the B3LYP/aug-cc-pVDZ level, the migrating hydrogen is 1.15 Å away from the origin (C atom), and 1.86 Å away from the migrating terminus (O atom). The P−O bond that is broken is surprisingly long at 2.34 Å. The CBS-QB3 barriers are 92.8 and 24.5 kcal/mol for conformer II → TS4 → P4 + H_2 and P4 → TS8 → P5 + CO, respectively.

3. Reactions Derived from Conformer III. There are three feasible pathways from conformer III:

$$\text{Path 5: Conformer III} \rightarrow \text{TS5} \rightarrow \text{Isom1}$$

$$\text{Path 6: Conformer III} \rightarrow \text{TS6} \rightarrow \text{P1} + CH_3OH$$

$$\text{Path 7: Conformer III} \rightarrow \text{TS7} \rightarrow \text{P3} + CH_3OH$$

As shown in Figure 1 and Figure 4, path 5 is a simple H shift from the C atom of a CH_3 group to the O atom of P═O leading to Isom1. The CBS-QB3 barrier for this process is 61.1

TABLE 2: B3LYP, MPW1K, and MP2 Harmonic Frequencies for Conformer II and TS3[a]

B3LYP	MPW1K	MP2
Conformer II		
12	22	23
62	65	78
97	114	93
121	134	129
167	180	173
196	207	206
206	215	212
255	268	261
292	301	296
355	376	364
444	466	445
486	508	494
675	728	694
753	806	768
785	831	813
896	919	895
916	940	915
1039	1123	1046
1066	1150	1071
1162	1201	1174
1162	1202	1174
1183	1227	1191
1188	1229	1198
1206	1266	1215
1305	1342	1312
1426	1457	1441
1428	1460	1443
1442	1484	1455
1448	1489	1462
1469	1510	1492
1475	1516	1498
1476	1517	1500
1481	1523	1505
3032	3113	3074
3035	3116	3077
3063	3140	3094
3114	3206	3173
3116	3208	3175
3144	3234	3207
3144	3236	3207
3162	3254	3212
3162	3254	3212
TS3		
626i	719i	782i
41	73	81
77	84	82
81	97	98
138	148	144
156	178	166
188	192	194
238	247	238
286	295	288
368	388	373
412	444	429
435	459	464
480	504	483
705	757	722
770	820	793
808	877	865
829	883	881
889	923	903
903	928	911
1038	1107	1039
1061	1145	1055
1077	1155	1115
1163	1202	1172
1186	1226	1193
1193	1263	1243
1298	1336	1305
1394	1426	1422
1424	1457	1439
1428	1461	1442
1444	1485	1452
1446	1488	1490
1470	1509	1491
1481	1522	1504
3026	3106	3064
3061	3139	3087
3101	3193	3152
3139	3214	3157
3144	3229	3199
3159	3250	3203
3160	3251	3204
3314	3387	3306
3322	3404	3331

[a] The aug-cc-pVDZ basis set was used for the calculations.

TABLE 3: B3LYP/aug-cc-pVDZ, MPW1K/aug-cc-pVDZ, MP2/aug-cc-pVDZ, and CBS-QB3 Relative Energies (kcal/mol) for Stationary Points on the DMMP PES

structure	B3LYP	MPW1K	MP2	CBS-QB3
conformer I	0	0	0	0
conformer II	0.0	0.1	0.2	0.4
conformer III and IV	2.1	2.1	1.6	1.9
Isom1	40.2	40.2	41.1	42.8
Isom2	46.3	44.2	44.2	48.7
Im1	86.3	91.2	88.7	87.7
P1 + CH_3OH	58.2	66.5	66.7	70.7
P2 + CH_2	99.1	104.4	104.7	94.3
P3 + CH_3OH	50.8	54.6	57.0	59.7
P4 + H_2	88.3	95.9	93.2	81.7
P5 + H_2 + CO	43.0	55.8	48.7	51.4
TS1	63.0	63.0	63.3	62.9
TS2	89.9	95.9	93.2	89.7
TS3	58.0	65.8	61.7	59.1
TS4	94.2	101.2	100.8	93.2
TS5	62.7	64.0	63.4	63.0
TS6	67.4	71.8	68.1	73.2
TS7	85.2	89.4	84.5	90.4
TS8 + H_2	101.4	123.1	108.6	106.2

[a] The standard deviations of the B3LYP, MPW1K, and MP2 energies are 4.6, 6.2, and 4.9 kcal/mol, respectively.

kcal/mol. As shown in Figure 1, TS5 has a loose POHC four-membered ring structure, whose B3LYP/aug-cc-pVDZ geometry is slightly nonplanar with a dihedral angle of 2.1°. The distance of the forming O−H bond is 1.24 Å, while that of the C−H bond that is broken is 1.60 Å.

Both paths 6 and 7 involve C−H and P−O bond cleavages accompanied by O−H bond formation through transition states TS6 and TS7, respectively. Conformer III dissociates to CH_3OH. The difference between the two paths is that the migrating hydrogen is from the methyl group for TS6, whereas for TS7 it is from a methoxy group. The CBS-QB3 dissociation barriers are 71.3 and 88.5 kcal/mol for paths 6 and 7, respectively. In TS6 and TS7, the respective forming O−H bond lengths are 1.13 and 1.09 Å, while the breaking P−O distances are 1.95 and 2.04 Å. TS6 has a four-membered ring structure, which is slightly nonplanar with a B3LYP/aug-cc-pVDZ dihedral angle of 5.2°. In TS7, besides O−H bond formation and P−O bond breakage as in TS6, a new P−C bond is formed with a bond distance of 2.15 Å. Therefore, the structures of P1 and P3 are quite different. P1 is planar, while P3 has a three-membered ring.

D. Reaction Mechanisms. As presented above, seven reaction channels are found for the gas-phase unimolecular decomposition of DMMP, and it is of interest to consider the expected mechanism(s) for the thermal gas-phase dissociation of DMMP. DMMP has three conformers, conformers I−III, which are formed by an internal rotation about a P−O bond. These three species have similar potential energies but different dissociation channels as shown in Figure 4. DMMP has two additional isomers in which a H atom is transferred to the O atom of the P═O bond, that is, Isom1and Isom2. No decomposition paths were found from these two isomers.

The overall barrier heights for the pathways from a DMMP conformer to products or another DMMP isomer are slightly dependent on the level of theory, as shown below for the aug-cc-pVDZ basis set:

CBS-QB3: TS3(59.1) < TS1(62.9) ≈ TS5(63.0) < TS6(73.2) < TS2(89.7) < TS7(90.4) < TS4(93.2)

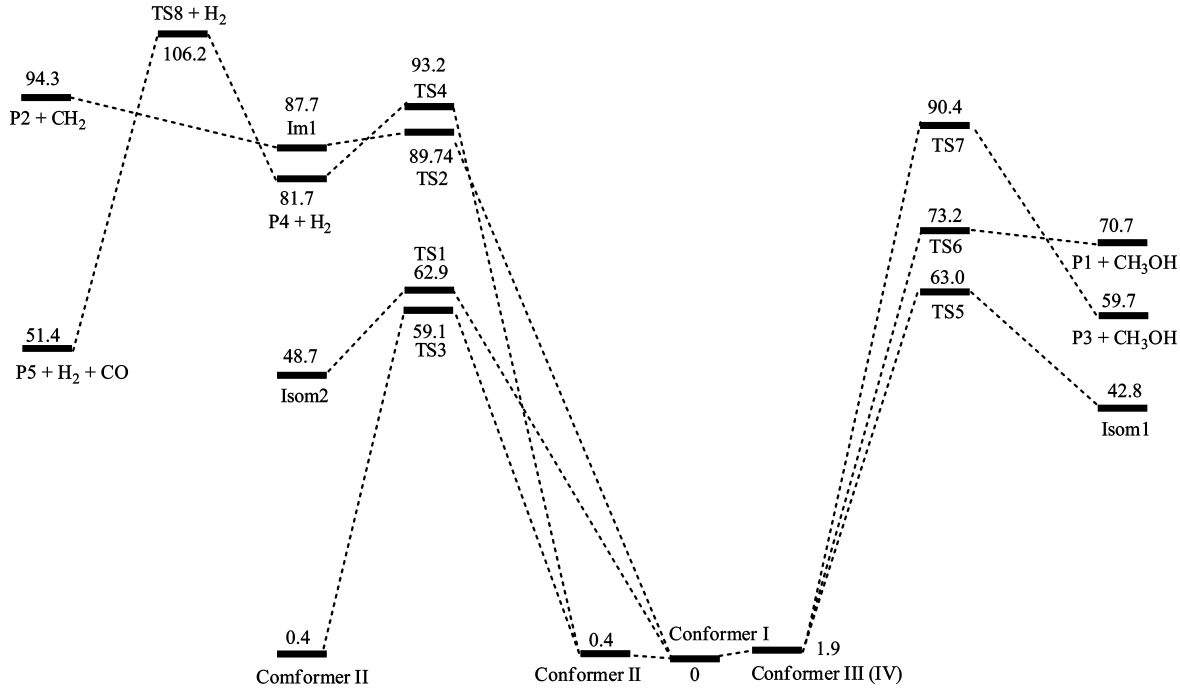

Figure 4. Energy profile (in kcal/mol) of the IRC-PES for DMMP unimolecular decomposition. The energies are the CBS-QB3 values.

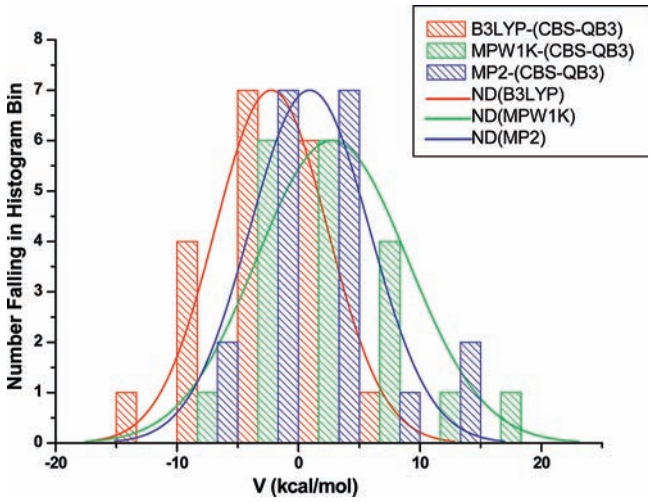

Figure 5. Histograms of differences between stationary point energies calculated with B3LYP, MPW1K, and MP2, employing the aug-cc-pVDZ basis set, and the CBS-QB3 values. Nineteen different stationary point energies are included in each of the histograms and each is fit with the normal distribution of error curve. The fitting parameters are given in the text.

MP2: TS3(61.7) < TS1(63.3) ≈ TS5(63.4) < TS6(68.1) < TS7(84.5) < TS2(93.2) < TS4(100.8)

MPW1K: TS1(63.0) ≈ TS5(64.0) < TS3(65.8) < TS6(71.9) < TS7(89.4) < TS2(96.0) < TS4(101.2)

B3LYP: TS3(58.0) < TS5(62.7) ≈ TS1(63.0) < TS6(67.4) < TS7(85.2) < TS2(89.9) < TS4(94.2)

For each theoretical method, the TS1 and TS5 energies differ by less than 1 kcal/mol. The energy for TS3 differs from those of TS1 and TS5 by less than 5 kcal/mol. The pathways for TS1, TS3, and TS5 involve isomerizations between the DMMP conformers. The lowest energy dissociation pathway is via TS6 to form P1, (O)P(CH_2)(OCH_3), + CH_3OH. There are several

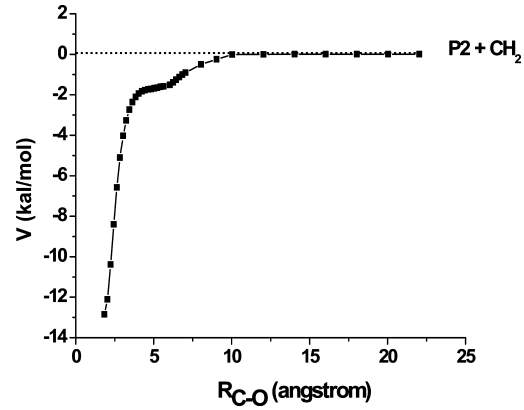

Figure 6. Dissociation curve of intermediate Im1 to the products P2 + CH_2 for DMMP unimolecular dissociation at the B3LYP/aug-cc-PVDZ level. *R* is the C−O distance (Å). *V* (kcal/mol) is the relative energy with respect to the products P2 + CH_2.

differences between the predictions of the different theoretical methods. For the CBS-QB3, B3LYP, and MP2 methods, the energy of TS3 is lower than those of TS1 and TS5, whereas for the MPW1K method, it is higher. In comparing the higher energy dissociation pathways, for the MP2, MPW1K, and B3LYP methods, the TS7 energy is lower than that of TS2, but for the CBS-QB3 method, it is slightly higher than TS2 and lower than TS4.

In an extensive study, Zheng et al.[39] compared different theoretical methods and basis sets for calculating barrier heights for chemical reactions. Their calculations were performed for a representative set of heavy atom transfer, nucleophilic substitution, unimolecular and association, and hydrogen transfer reactions. Their benchmark energies came from experiment and Weizmann-1[40] and Weizmann-2[41] calculations. The latter are combined CCSD and CCSD(T) calculations with large basis sets. Energies from different electron structure theories were compared with these benchmark values. They compared CBS-QB3 and MP2, MPW1K, and B3LYP, with the 6-31+G (d,p) basis sets and found that their mean unsigned errors in the barrier heights of the representative set of reactions for CBS-QB3, MP2,

MPW1K, and B3LYP are 1.56, 6.25, 1.92, and 4.84 kcal/mol. The CBS-QB3 and MPW1K/6-31+G (d,p) methods were found to have similar accuracies, with MP2/6-31+G (d,p) giving considerably less accurate barrier heights.

This near equivalence between CBS-QB3 and MPW1K is not found for the stationary point energies reported here for phosphorus containing compounds. As shown in Figure 5 for the transition states and potential minima of the phosphorus containing compounds, the MP2 and B3LYP energies with the aug-cc-pVDZ basis set are in better agreement with the CBS-QB3 values than are the MPW1K/aug-cc-pVDZ energies.

IV. Summary

This work investigated geometries, frequencies, and energies of the reactants, isomers, intermediates, transition states, and products and mechanisms for the unimolecular decomposition of gas-phase DMMP. The B3LYP, MPW1K, MP2 and CBS-QB3 theories were used for the quantum chemical calculations. The effect of basis set size was also considered. The results show that the variations in bond distances, caused by changing the basis set, are relatively small for most of the stationary points. Bond angle differences depend on the stationary point and calculation methods and range from 0° to 7.8°. Overall, the geometries calculated at the different levels of theory are in good agreement. For the aug-cc-pVDZ basis set, the primary geometry differences obtained by the functionals B3LYP and MPW1K lie in the bond angles of the transition state TS7 (2.6°) and TS5 (2.5°). Also, the largest variation in the DFT and MP2 geometries is 5.9° for the bond angle P−O3−C3 of Im1.

CBS-QB3 energies were chosen as a benchmark for the accuracy of the calculations and were compared with energies calculated with MP2, B3LYP, and MPW1K. For the DMMP unimolecular decomposition pathways, the energy barriers for the isomerization processes, that is, channels 1 and 5, are nearly the same at all levels of theory, and lower than the barriers for the dissociation processes, that is, channels 6, 2, 7, and 4. Four different products, P1, P2, P3, and P4, whose structures are given in Figure 1, are observed. Among these products, P1 is the most favorable with a CBS-QB3 barrier for formation of 71.3 kcal/mol. The formation of P2, P3, and P4 are predicted to be competitive, because the barriers for their formation are similar. The product P4 forms a fifth product, P5, by a secondary reaction.

Finally, it is important to emphasize that the reaction mechanisms identified here are for gas-phase DMMP and provide an understanding of DMMP decomposition in the absence of a catalyst. A catalyst such as TiO_2(s) will lower the barrier height for DMMP decomposition and, in addition, possibly the decomposition pathways. Calculations are planned to study the catalytic decomposition of DMMP, and it will be of interest to determine the extent of similarity with the gas-phase decomposition.

Acknowledgment. This material is based upon work supported by the Army Research Office under Contract No. HDTRA1-07-C-0098 and the Robert A. Welch Foundation under Grant D-0005. Support was also provided by the High-Performance Computing Center (HPCC) at Texas Tech University, under the direction of Dr. Philip W. Smith.

Supporting Information Available: Geometries and frequencies of stationary points. This material is available free of charge via the Internet at http://pubs.acs.org.

References and Notes

(1) Mitchell, M. B.; Sheinker, V. N.; Tesfamichael, A. B.; Gatimu, E. N.; Nunley, M. *J. Phys. Chem. B* **2003**, *107*, 580.
(2) Segal, S. R.; Suib, S. L.; Tang, X.; Satyapal, S. *Chem. Mater.* **1999**, *11*, 1687.
(3) Trubitsyn, D. A.; Vorontsov, A. V. *J. Phys. Chem. B* **2005**, *109*, 21884.
(4) Nassar, A. F.; Lucas, S. V.; Jones, W. R.; Hoffland, L. D. *Anal. Chem.* **1998**, *70*, 1085.
(5) Knagge, K.; Johnson, M.; Grassian, V. H.; Larsen, S. C. *Langmuir* **2006**, *22*, 11077.
(6) Panayotov, D. A.; Morris, J. R. *J. Phys. Chem. C* **2008**, *112*, 7496.
(7) Smentkowski, V. S.; Hagans, P.; Yates, J. T., Jr. *J. Phys. Chem.* **1988**, *92*, 6351.
(8) Cuisset, A.; Mouret, G.; Pirali, O.; Roy, P.; Cazier, F.; Nouali, H.; Demaison, J. *J. Phys. Chem. B* **2008**, *112*, 12516.
(9) Tzou, T. Z.; Weller, S. W. *J. Catal.* **1994**, *146*, 370.
(10) Templeton, M. K.; Weinberg, W. H. *J. Am. Chem. Soc.* **1985**, *107*, 97.
(11) Henderson, M. A.; Jin, T.; White, J. M. *J. Phys. Chem.* **1986**, *90*, 4607.
(12) Hedge, R. M.; White, J. M. *Appl. Surf. Sci.* **1987**, *28*, 1.
(13) Hegde, R. I.; Greenlief, C. M.; White, J. M. *J. Phys. Chem.* **1985**, *89*, 2886.
(14) Henderson, M. A.; White, J. M. *J. Am. Chem. Soc.* **1988**, *110*, 6939.
(15) Guo, X.; Yoshinobu, J.; Yates, J. T., Jr. *J. Phys. Chem.* **1990**, *94*, 6839.
(16) Rusu, C. N.; Yates, J. T., Jr. *J. Phys. Chem. B* **2000**, *104*, 12299.
(17) Moss, J. A.; Szczepankiewicz, S. H.; Park, E.; Hoffmann, M. R. *J. Phys. Chem. B* **2005**, *109*, 19779.
(18) Templeton, M. K.; Weinberg, W. H. *J. Am. Chem. Soc.* **1985**, *107*, 774.
(19) Li, Y; Schlup, J. R.; Klabunde, K. J. *Langmuir* **1991**, *7*, 1394.
(20) Lin, S.-T.; Klabunde, K. J. *Langmuir* **1985**, *1*, 600.
(21) Gordon, W. O.; Tissue, B. M.; Morris, J. R. *J. Phys. Chem. C* **2007**, *111*, 3233.
(22) Tesfai, T. M.; Sheinker, V. N.; Mitchell, M. B. *J. Phys. Chem.* **1998**, *102*, 7299.
(23) Bermudez, V. M. *J. Phys. Chem. C* **2007**, *111*, 3719.
(24) Bermudez, V. M. *Surf. Sci.* **2008**, *602*, 1938.
(25) Bermudez, V. M. *J. Phys. Chem. C* **2009**, *113*, 1917.
(26) Bermudez, V. M. *J. Phys. Chem. C* **2007**, *111*, 9314.
(27) Werner, J. H.; Cool, T. A. *Combust. Flame* **1999**, *117*, 78.
(28) Zheng, F.; Zhan, C. G.; Ornstein, R. L. *J. Chem. Soc., Perkin Trans. 2* **2001**, 2355.
(29) Šečkutė, J.; Menke, J. L.; Emnett, R. J.; Patterson, E. V.; Cramer, C. J. *J. Org. Chem.* **2005**, *70*, 8649.
(30) (a) Møller, C.; Plesset, M. S. *Phys. ReV.* **1934**, *46*, 618. (b) Pople, J. A.; Binkley, J. S.; Seeger, R. *Int. J. Quantum Chem. Symp.* **1976**, *10*, 1. (c) Pople, J. A.; Krishnan, R.; Schlegel, H. B.; Binkley, J. S. *Int. J. Quantum Chem. Symp.* **1979**, *13*, 325. (d) Handy, N. C.; Schaefer, H. F. III *J. Chem. Phys.* **1984**, *81*, 5031.
(31) (a) Becke, A. D. *J. Chem. Phys.* **1993**, *98*, 5648. (b) Lee, C.; Yang, W.; Parr, R. *Phys. Rev. B* **1988**, *37*, 785. (c) Kohn, W.; Becke, A. D.; Parr, R. *J. Phys. Chem.* **1996**, *100*, 12974.
(32) (a) Adamo, C.; Barone, V. *J. Chem. Phys.* **1998**, *108*, 664. (b) Rey, J.; Savin, A. *Int. J. Quantum Chem.* **1998**, *69*, 581.
(33) (a) Woon, D. E.; Dunning, T. H. *J. Chem. Phys.* **1993**, *98*, 1358. (b) Dunning, T. H. *J. Chem. Phys.* **1989**, *90*, 1007.
(34) Fukui, K. *Acc. Chem. Res.* **1981**, *14*, 363.
(35) (a) Montgomery, J. A., Jr.; Frisch, M. J.; Ochterski, J. W.; Petersson, G. A. *J. Chem. Phys.* **2000**, *112*, 6532. (b) Montgomery, J. A., Jr.; Frisch, M. J.; Ochterski, J. W.; Petersson, G. A. *J. Chem. Phys.* **1999**, *110*, 2822.
(36) (a) Bylaska, E. J.; de Jong, W. A.; Govind, N.; Kowalski, K.; Straatsma, T. P.; Valiev, M.; Wang, D.; Apra, E.; Windus, T. L.; Hammond, J.; Nichols, P.; Hirata, S.; Hackler, M. T.; Zhao, Y.; Fan, P.-D.; Harrison, R. J.; Dupuis, M.; Smith, D. M. A.; Nieplocha, J.; Tipparaju, V.; Krishnan, M.; Wu, Q.; Van Voorhis, T.; Auer, A. A.; Nooijen, M.; Brown, E.; Cisneros, G.; Fann, G. I.; Fruchtl, H.; Garza, J.; Hirao, K.; Kendall, R.; Nichols, J. A.; Tsemekhman, K.; Wolinski, K.; Anchell, J.; Bernholdt, D.; Borowski, P.; Clark, T.; Clerc, D.; Dachsel, H.; Deegan, M.; Dyall, K.; Elwood, D.; Glendening, E.; Gutowski, M.; Hess, A.; Jaffe, J.; Johnson, B.; Ju, J.; Kobayashi, R.; Kutteh, R.; Lin, Z.; Littlefield, R.; Long, X.; Meng, B.; Nakajima, T.; Niu, S.; Pollack, L.; Rosing, M.; Sandrone, G.; Stave, M.; Taylor, H.; Thomas, G.; van Lenthe, J.; Wong, A.; Zhang, Z. *NWChem, A Computational Chemistry Package for Parallel Computers, Version 5.1*; Pacific Northwest National Laboratory: Richland, Washington 99352−0999, 2007. (b) Kendall, R. A.; Apra, E.; Bernholdt, D. E.; Bylaska, E. J.; Dupuis, M.; Fann, G. I.; Harrison, R. J.; Ju, J.; Nichols, J. A.; Nieplocha, J.; Straatsma, T. P.; Windus, T. L.; Wong, A. T. High Performance Computational Chemistry: An Overview of NWChem a Distributed Parallel Application. *Comput. Phys. Commun.* **2000**, *128*, 260–283.

(37) Frisch, M. J.; Trucks, G. W.; Schlegel, H. B.; Scuseria, G. E.; Robb, M. A.; Cheeseman, J. R. ; Montgomery J. A., Jr.; Vreven, T.; Kudin, K. N.; Burant, J. C.; Millam, J. M.; Iyengar, S. S.; Tomasi, J.; Barone, V.; Mennucci, B.; Cossi, M.; Scalmani, G.; Rega, N.; Petersson, G. A.; Nakatsuji, H.; Hada, M.; Ehara, M.; Toyota, K.; Fukuda, R.; Hasegawa, J.; Ishida, M.; Nakajima, T.; Honda, Y.; Kitao, O.; Nakai, H.; Klene, M.; Li, X.; Knox, J. E.; Hratchian, H. P.; Cross, J. B.; Bakken, V.; Adamo, C.; Jaramillo, J.; Gomperts, R.; Stratmann, R. E.; Yazyev, O.; Austin, A. J.; Cammi, R.; Pomelli, C.; Ochterski, J. W.; Ayala, P. Y.; Morokuma, K.; Voth, G. A.; Salvador, P.; Dannenberg, J. J.; Zakrzewski, V. G.; Dapprich, S.; Daniels, A. D.; Strain, M. C.; Farkas, O.; Malick, D. K.; Rabuck, A. D.; Raghavachari, K.; Foresman, J. B.; Ortiz, J. V.; Cui, Q.; Baboul, A. G.; Clifford, S.; Cioslowski, J.; Stefanov, B. B.; Liu, G.; Liashenko, A.; Piskorz, P.; Komaromi, I.; Martin, R. L.; Fox, D. J.; Keith, T.; Al.Laham, M. A.; Peng, C. Y.; Nanayakkara, A.; Challacombe, M.; Gill, P. M. W.; Johnson, B.; Chen, W.; Wong, M. W.; Gonzalez, C.; Pople, J. A. *Gaussian 03, Revision B.04*; Gaussian, Inc.: Pittsburgh, PA, 2003.

(38) Suenram, R. D.; Lovas, F. J.; Plusquellic, D. F.; Lesarri, A.; Kawashima, Y.; Jensen, J. O.; Samuels, A. *J. Mol. Spectrosc.* **2002**, *211*, 110.

(39) Zheng, J. J.; Zhao, Y.; Truhlar, D. G. *J. Chem. Theory Comput.* **2007**, *3*, 569.

(40) Martin, J. M. L.; de Oliveira, G. *J. Chem. Phys.* **1999**, *111*, 1843.

(41) Parthiban, S.; de Oliveira, G.; Martin, J. M. L. *J. Phys. Chem. A* **2001**, *105*, 895.

JP904232N